Polarized Raman spectroscopy of v-SiO_2 under rare-gas compression

C. Weigel,[1] M. Foret,[1,*] B. Hehlen,[1] M. Kint,[1] S. Clément,[1] A. Polian,[2] R. Vacher,[1] and B. Rufflé[1]
[1]*Laboratoire Charles Coulomb (L2C), UMR 5221 CNRS-Université de Montpellier, F-34095 Montpellier, France*
[2]*Sorbonne Universités, UPMC Université Paris 6 and CNRS, UMR 7590, IMPMC, F-75005 Paris, France*
(Received 22 April 2016; revised manuscript received 31 May 2016; published 20 June 2016)

High-pressure polarized Raman spectra of vitreous silica are measured up to 8 GPa in a diamond-anvil cell at room temperature. The combined use of either a nonpenetrating pressurizing medium—argon—or a penetrating one—helium, allows one to separate density from stress effects on the Raman frequencies. In the framework of a simple central force model, the results emphasize the distinct role played by the shrinkage of the intertetrahedral angle Si-O-Si and the force-constant stiffening during the compression. The polarization analysis further reveals the existence of an additional isotropic component in the high-frequency wing of the boson peak. The pressure dependence of the genuine boson peak frequency is found to be much weaker than previously reported and even goes through a minimum around 2 GPa in remarkable coincidence with the anomalous compressibility maximum of silica.

DOI: 10.1103/PhysRevB.93.224303

I. INTRODUCTION

Vitreous silica v-SiO_2 is a material of both fundamental—as it is an archetypal network forming glass—and technological interest—as it is widely used in optical and electronic devices. Its behavior under pressure is of long-standing interest due to its importance as the analog material of silicate melts in geophysics. Silica glass presents remarkable properties when submitted to high pressure P. For instance, it can be permanently compacted up to a densification rate of 20%, leading to a disordered solid for which the density is comparable to that of quartz [1,2]. It also shows an anomalous mechanical behavior at high P: from ambient P to 2 GPa, its compressibility increases, then decreases above 2 GPa as expected for most solids [3]. These unusual features have been linked to the existence of a large interstitial free volume fraction of v-SiO_2 allowing strong structural modifications with P [4–8]. It is also well known that rare gases can diffuse into the open structure of v-SiO_2, at different rates and in variable quantities according to their atomic sizes [9], e.g., 0.1 mole of He per mole of SiO_2 is expected to be incorporated in the interstitial sites of the network. However, it has been shown recently that unexpected greater amounts of fluid could be adsorbed into the vitreous matrix pressurized in He [10,11], up to nearly 1 mole of He per mole of SiO_2 at 6 GPa. Moreover, it is also found out that the compressibility anomaly is suppressed concomitantly with He incorporation into the network [12,13]. All this stems from the unique intertetrahedral flexibility of the silica network allowing deformation and compaction of the interstitial voids [14–16]. There is a great interest in establishing the precise related structural evolutions of the network, which may extend across the medium-range structure of the glass [17–19]. Gas solubility itself is also important to understand how the glass properties can be modified by ion exchange, e.g., in nuclear waste glasses. In melts, gas solubility impacts the synthesis methods in the glass industry and it is also of great concern for the geophysical community as well. The complex interplay between gas adsorption, mechanical properties, and structural evolutions at high P is far from being fully understood.

In this work, *in situ* Raman scattering is used to investigate the compression mechanisms of silica glass under purely hydrostatic loading in the 0–8 GPa range. Silica samples are pressurized in two different rare gases: a penetrating one (He) and a nonpenetrating one (Ar). Investigating silica under both pressurizing fluids allows varying SiO_2 skeleton density irrespective of fluid pressure. The Ar- and He-pressure evolution of Raman frequencies are analyzed using a simple central force model [20], allowing one to disentangle the role of the intertetrahedral Si-O-Si angle from the Si-O force constant on the compression process. Further, a polarization analysis is performed at high pressure in both media. It highlights the presence of an additional component on the high-frequency tail of the ubiquitous boson peak. The former being essentially active in VV, the VH spectra provides therefore the actual P dependence of the boson peak. Its frequency exhibits a minimum around 2 GPa, concurring with the elastic anomaly, a behavior markedly different from previous results obtained without polarization analysis [21–23]. In Sec. II, we describe our experimental arrangement. Our measurements are presented together with the data analysis in Sec. III and we discuss our findings in Sec. IV. A summary is presented in Sec. V.

II. MATERIAL AND METHODS

A. Sample and experimental setup

The *in situ* high-pressure measurements are performed in Chervin-type diamond-anvil cells [24], equipped with diamonds of 800 μm culet size. The samples are platelets of Suprasil F300 ([OH] $<$ 1 ppm) from Heraeus Quartzglass, Germany, of thickness $e_{SiO_2} = 56$ μm, and of lateral dimensions about 100 μm. The plate surfaces are of optical quality. They are loaded in chambers of 400 μm diameter and 200 μm thickness drilled in rhenium gaskets. The hydrostatic pressure is applied up to 8 GPa at room temperature using either argon as a nonpenetrating pressure-transmitting medium or helium as a penetrating one. The pressure is determined using the fluorescence of a ruby gauge [25].

The Raman spectra are measured using a solid laser emitting at $\lambda_0 = 532$ nm. The scattered light is analyzed in backscattering geometry using a Jobin-Yvon FHR-640

*Corresponding author: marie.foret@umontpellier.fr

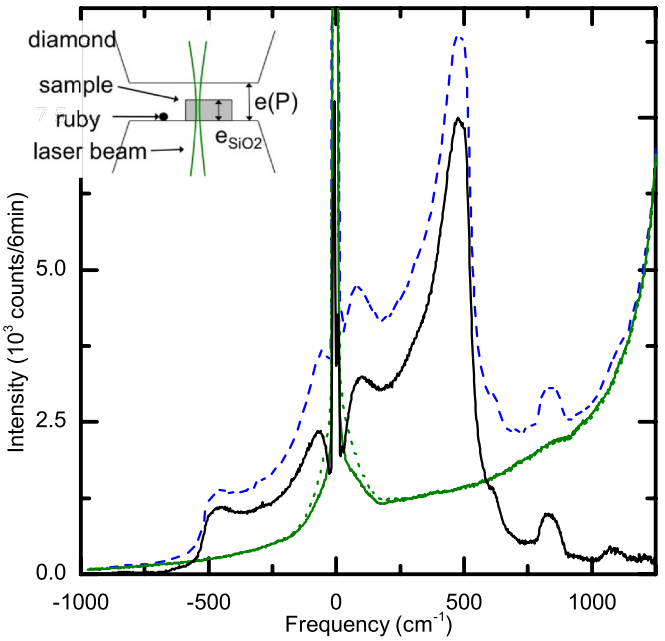

FIG. 1. VV Raman intensity at 7.0 GPa under He pressure. The blue dashed and green dotted lines represent the measured I_{samp} and γI_{DAC} spectra, respectively ($\gamma = 0.98$). The green solid line is γI_{DAC} corrected for the excess He fluid low-frequency contribution. The black solid line is the resulting spectrum of the SiO_2 sample, I^{RS}. Inset: schematics of the sample chamber.

single-grating (600 grooves/mm) diffractometer. Using an entrance slit of 100 μm, a resolution of $\sim$6 cm^{-1} (full width at half maximum) is achieved. The light is focused into the sample and collected using a confocal microscope with a $\times$20 objective. The focused laser beam on the sample has a waist of $\sim$10 μm and a depth of focus of $\sim$250 μm. The elastically scattered light is filtered using three combined Bragg bandstop filters followed by a spatial filter, giving access to both Stokes and anti-Stokes scattering. Under mechanical stress, the diamond anvils alter the polarization state of the incident and scattered light, which is restored using a Soleil-Babinet compensator introduced before the microscope. The polarization of the scattered light is then analyzed with a wideband half-wave plate combined with a large aperture Glan polarizer.

B. Treatment of raw data

The treatment aims at removing the parasitic contributions of the diamond anvils and of the pressurizing fluid from the raw data. Let I_{samp} and I_{DAC} be the intensities collected at pressure P consecutively with the laser beam focused into the chamber, inside and outside the sample, respectively (see the sketch in Fig. 1). Typical I_{samp} and γI_{DAC} spectra measured in VV polarization at 7.0 GPa in He are shown in Fig. 1 as a blue dashed line and a green dotted line, respectively. γ is a scaling factor, close to 1, introduced to take into account inherent variations of settings when measuring I_{samp} and I_{DAC}. Both spectra contain the same amount of signal scattered by the diamond anvils (i.e., an intense band [26] at 1332 cm^{-1} and a small multiphonon contribution at $|\omega| \leqslant 200\,\text{cm}^{-1}$). They include, however, variable amounts of quasielastic signal from the fluid, depending on the relative thicknesses of the silica sample e_{SiO_2} and of the DAC chamber $e(P)$. Therefore, the proper Raman spectra of v-SiO_2 at low frequency cannot be simply obtained subtracting γI_{DAC} from I_{samp}. The magnitude of the scattering due to the rare gas alone in I_{DAC} is estimated by removing the diamond spectrum (evaluated independently) from I_{DAC}. For He gas, it amounts to about 10% of I_{DAC} at low frequency. Provided that $e(P)$ and e_{SiO_2} are known, the *excess* He fluid contribution is properly subtracted from I_{DAC} (green solid line in Fig. 1) and the accurate Raman spectrum of the silica sample I^{RS} is obtained (black solid line). Ar is in a fluid phase up to $\sim$1.3 GPa and its scattering turns out to be very intense due to its large atomic polarizability, even exceeding that of the sample. The low-frequency region of those spectra is therefore left out of the analysis. Ar crystallizes into a soft fcc crystal [27] at $\sim$1.3 GPa leaving only a weak second-order Raman signal [28] that is negligible in our experiments.

III. RESULTS

The Raman signal is proportional to the space and time Fourier transform of the correlation function of the first-order polarization. The contribution of a molecular vibrational mode σ to Raman scattering intensity reads [29]

$$I^{\text{RS}}(\omega) \propto \frac{V\omega_i\omega_s^3}{\omega} C_\sigma [n(\omega)+1] g_\sigma(\omega), \tag{1}$$

where ω_i and ω_s are the incoming and outgoing photon angular frequencies, respectively, $\omega = \omega_i - \omega_s$ is the exchanged frequency, V is the scattering volume, n is the Bose-Einstein population number, and $g_\sigma(\omega)$ is the spectral response of the mode, which in glasses refers to its density of states [30]. C_σ is the coupling-to-light coefficient of the mode σ. For scattering by an isotropic molecular medium, C_σ is an isotropic average over the polarizability tensor elements associated to mode σ. C_σ depends on the polarization geometry—VV when the incident- and scattered-light polarization vectors are parallel, or VH when they are perpendicular. In glasses, the Raman response results in inhomogeneously broadened bands owing to structural disorder [30]. Furthermore, the coupling-to-light coefficient might be frequency dependent within the modes of a particular band [31,32]. In the following, we make use of the usual effective relation for the reduced Raman intensity:

$$I_{\text{red}}(\omega) = \frac{1}{\rho\omega_s^3} \frac{I^{\text{RS}}(\omega)}{\omega[n(\omega)+1]} \propto C(\omega)\frac{g(\omega)}{\omega^2}. \tag{2}$$

This data reduction removes the temperature effect from I^{RS} without loss of spectral information at low frequencies. As the scattering volume remains constant in every change of pressure, it is worthwhile to normalize with respect to the density of the sample, ρ. With this proper normalization, it turns out that the total integrated VV intensity over the available frequency range, $I_{\text{tot}}^{\text{VV}} = \int_{25}^{1160} I_{\text{red}}^{\text{VV}}(\omega)d\omega$, stays nearly constant upon compression for both pressurizing media. We thus normalize the VV intensities to the appropriate $I_{\text{tot}}^{\text{VV}}$. Due to the unequal transmission of VV- and VH-polarized light through the microscope it remains difficult to obtain accurate relative VH intensities as a function of P. Therefore, an increasing small drift of the relative VH intensities with P

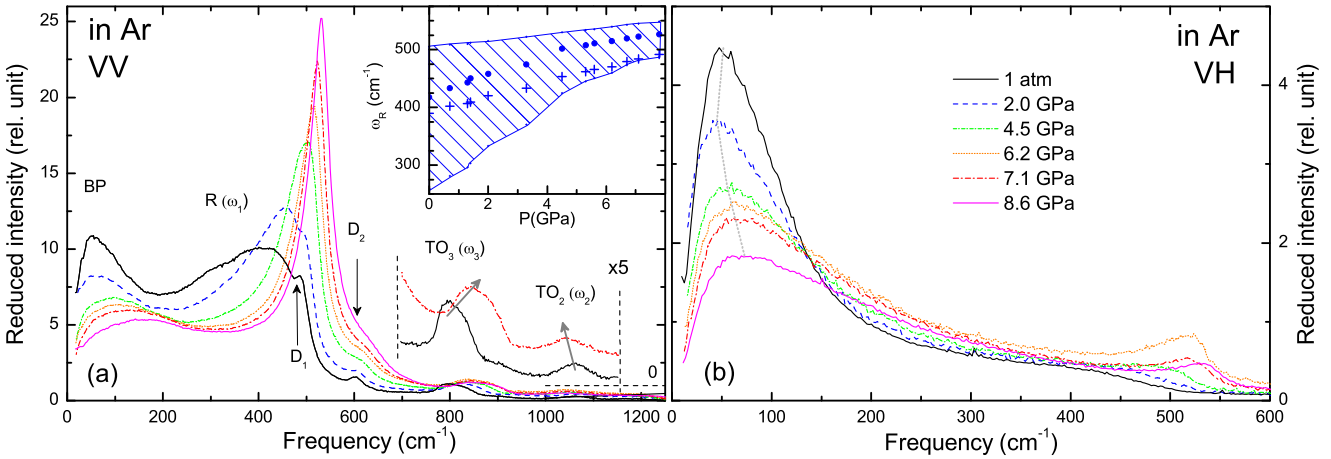

FIG. 2. Polarized VV (a) and depolarized VH (b) contributions to the reduced spectra of v-SiO_2 at some selected argon pressure. The upper inset shows the frequencies of the maximum (circles), of the mean (crosses) of the R band and its full width at half maximum (striped area). The lower inset shows some selected spectra amplified by a factor 5 (the arrows emphasize the pressure shifts with opposite sign for the TO_3 and TO_2 lines). Note the different X and Y scales between figures (a) and (b).

cannot be excluded. We present in Figs. 2 and 3 the VV and VH reduced and normalized spectra at few selected pressures of Ar and He, respectively.

The assignment of the Raman bands of v-SiO_2 is well documented [32–35]. The VV spectrum at ambient pressure [black lines in Figs. 2(a) and 3(a)] shows a dominant, rather broad and highly polarized line centered around 400 cm^{-1} generally referred to as the R band. This band is mainly silent in the VH spectrum. The analysis in terms of molecular selection rules shows that the R band relates to the A_1-symmetry bending mode of the Si-O-Si unit in the tetrahedral network. This vibration involves oxygen-atom displacement along the Si-O-Si bisector in the plane of the structural unit [36]. In the small three- and four-membered rings (closed paths containing n Si-O segments are referred to as n-membered rings), those motions are in phase and decoupled from the network, resulting in the narrow D_2 and D_1 lines around 605 and 495 cm^{-1}, respectively [37,38].

It was early stated that the frequency distribution of these bands is associated with the spread of the intertetrahedral angle θ in the silica network [20,31,39]. A compilation of the most recent first-principles investigations [32,40] and analyses of diffraction [41,42] and NMR data [43] sets out a mean value of the Si-O-Si bond angle distribution to $\sim 149 \pm 11^\circ$. The θ angles in the $n = 4$ and $n = 3$ rings are smaller and less spread out than in the network [38], $\theta_{D_1} \sim 136^\circ$ and $\theta_{D_2} \sim 128^\circ$. Accurate theoretical modeling and access to the Raman coupling factor now make possible the computation of Raman spectra for valuable numerical samples in fair agreement with experimental spectra [32,40,44]. In particular, it has been shown that the relevant scalar Raman coupling factor associated with the O-bending motions varies across the θ angle [32], leading to the effective relation $C_{O_b} \propto \omega^2$ [45]. Hence, I_{red} is the more relevant quantity as it directly yields the Raman density of states of O-bending modes $g_b(\omega)$. Looking at Figs. 2(a) and 3(a), it is clear that the frequency distribution

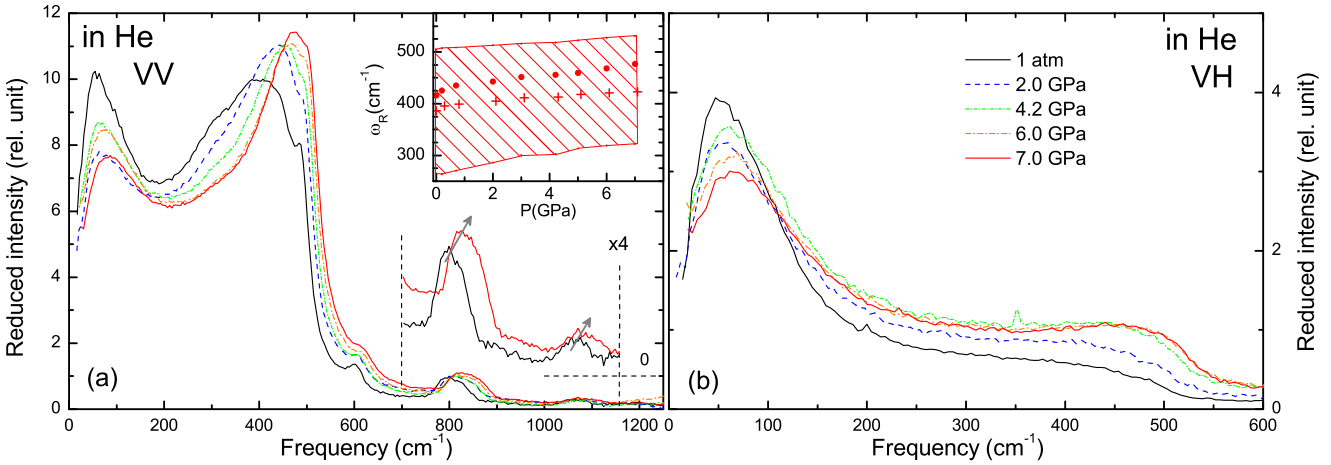

FIG. 3. Polarized VV (a) and depolarized VH (b) contributions to the reduced spectra of v-SiO_2 at some selected helium pressure. The upper inset shows the frequencies of the maximum (circles), of the mean (crosses) of the R-band, and its full width at half maximum (striped area). The lower inset shows some selected spectra amplified by a factor 4 (the arrows emphasize the positive pressure shift of both the TO_3 and TO_2 lines in He). Note the different X and Y scales between figures (a) and (b).

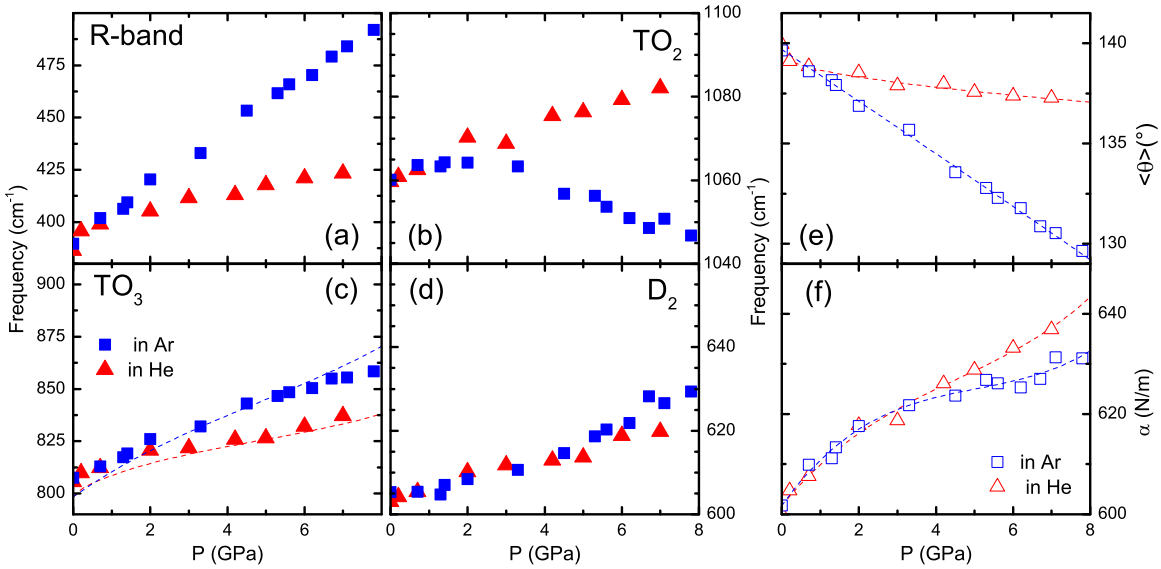

FIG. 4. Pressure dependence of the mean frequency of the Raman bands of VV spectra: (a) R band, (b) TO_2 line, (c) TO_3 line, and (d) D_2 line, using Ar (blue squares) and He (red triangles) as pressurizing media. Application of Eqs. (3a) and (3b) to the measured frequencies of the R band (ω_1) and TO_2 line (ω_2) gives the pressure dependencies of angle $\langle\theta(P)\rangle$ and force constant $\alpha(P)$ shown in panels (e) and (f), respectively. The dashed lines are splines to guide the eyes. The ω_3 values computed from these, using Eq. (3c), are shown as dashed lines in panel (c). Frequencies of TO_2 and TO_3 modes in VH spectra (not shown) are in good agreement with the ones presented here.

of the modes underlying the R band is strongly modified under Ar pressure, while it is much less upon He pressure. The insets show both the frequencies of the maximum (circles) and of the mean (crosses) of the distribution in addition to the full width at half maximum (striped area) of the R band in each case. One notices that the mean frequency is systematically lower than the frequency of the maximum, emphasizing its asymmetry. Under Ar pressure, a significant shift of the distribution to higher frequencies along with a strong narrowing occurs. Considerably weaker modifications are observed under He pressure. Concerning the D_1 band, its pressure evolution is not observable as it becomes rapidly buried in the intense R band with increasing P. The D_2 band slightly shifts to higher frequencies with increasing P in both pressurizing media.

At high frequencies, some of the polar modes of v-SiO_2, active in infrared absorption, also contribute to the Raman spectra. The transverse optical TO modes are labeled in Fig. 2(a) as in Ref. [46]. They are better described in the T_d point group of the SiO_4 tetrahedron and correspond to stretching motions of symmetry F_2 [36,47]. The high-frequency TO_1-TO_2 doublet, around 1200–1060 cm^{-1}, is well defined as mainly F_{2s} species ("asymmetric stretching"). It involves primarily oxygen motions [36]. TO_1 includes, however, a component of the symmetric breathing mode of the tetrahedron [47] but it will not be discussed here as this signal is buried in the tail of the intense Raman line of diamond. The TO_3 mode, around 808 cm^{-1}, has a mixed F_{2s} and F_{2b} (bending or symmetric stretching) character though dominated by bending [36,47]. Our data in Ar show that TO_3 follows a positive pressure shift, while it is found negative for TO_2 [zoom-in in Fig. 2(a)]. An opposite behavior applies to TO_2 when using He as pressurizing medium [zoom-in in Fig. 3(a)].

Finally, I_{red} exhibits a broadband in the 20–200 cm^{-1} range corresponding to the boson peak (BP) frequency region. BP is a universal feature of glasses associated to low-frequency excess modes over the Debye expectation. Their signature in Raman spectroscopy is controversial [48–50] and remains debated [51,52]. As far as we know, depolarized BP spectra of v-SiO_2 at varying pressure are collected here owing to the implementation of a compensation technique. We see evidence that the BP differs in VV and VH polarization under Ar compression as illustrated in Fig. 2. Furthermore, a slight negative pressure shift is apparent in the depolarized spectra at low pressure in Ar, while it is positive in He [see Figs. 2(b) and 3(b)]. We discuss in the following section the overall P behavior of all these main Raman lines.

IV. DISCUSSION

A. Molecular modes

Figures 4(a)–4(d) present the P dependence of the mean frequency of the Raman lines for both pressurizing fluids, Ar (blue squares) and He (red triangles). The overall P behavior of the modes can be rationalized with the help of a simple central-force model, developed by Sen and Thorpe in the 1970s to describe the dynamics of covalently bonded networks [20]. The model was early applied to the vibrational spectra of AX_2 tetrahedral glasses by Galeener [39]. It describes how the normal modes of an isolated AX_4 tetrahedron evolve into bandlike states due to the intertetrahedral coupling within the network. Treating only the nearest-neighbor central forces, the band limits are simply expressed as functions of the AXA bond angle θ, the A-X bond restoring force constant α, and the masses M and m of the cation A and the anion X, respectively [20]:

$$\omega_1^2 = (\alpha/m)(1+\cos\theta), \tag{3a}$$

$$\omega_2^2 = (\alpha/m)(1-\cos\theta), \tag{3b}$$

$$\omega_3^2 = \omega_1^2 + 4\alpha/3M, \tag{3c}$$

$$\omega_4^2 = \omega_2^2 + 4\alpha/3M. \tag{3d}$$

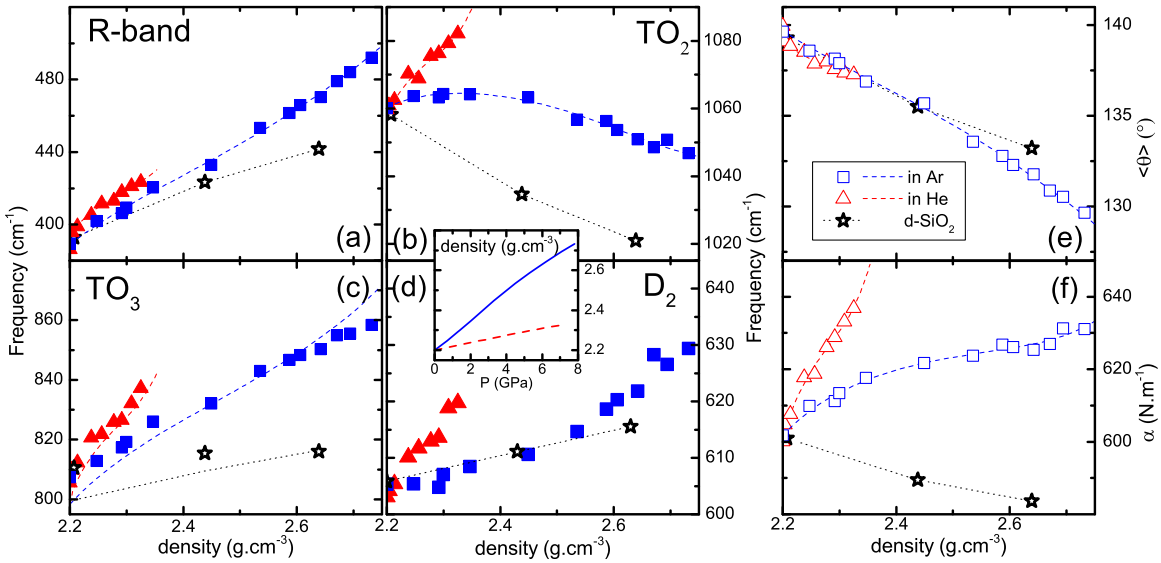

FIG. 5. Mean frequency of the Raman bands of VV spectra as a function of the SiO_2 skeleton density (ρ_{SiO_2}): (a) R band, (b) TO_2 line, (c) TO_3 line, and (d) D_2 line, using Ar (blue squares) and He (red triangles) as pressurizing media. The $\langle\theta\rangle$ angle and force constant α as a function of ρ_{SiO_2} are shown in panels (e) and (f), respectively. Lines are as in Fig. 4. Corresponding data for a series of permanently densified silica, d-SiO_2 [45,54], are also plotted (black stars; the dotted lines are guides for the eye). The inset represents ρ_{SiO_2} as a function of P under Ar (solid line) and He (dashed line) compression [12,13].

For $\theta = 90°$, one gets the modes of an isolated tetrahedron (singlet at $\omega^2 = \alpha/m$ and triplet at $\omega^2 = \alpha/m + 4\alpha/3M$). As θ increases from 90°, the molecular modes evolve into bands delineated by the above frequencies. In fact, the term $\cos\theta$ appears as an effective coupling constant [53] which is zero if $\theta = 90°$. The ω_1 frequency is associated to the pure bending motion of the anion, whereas ω_2 is pure stretching. In the following, as suggested by Galeener [34], we identify the main Raman features to the vibrational bands calculated by Sen and Thorpe. The masses m and M are fixed to those of O and Si atoms, respectively. Solving Eqs. (3a) and (3b) in terms of the measured frequencies of the R band (ω_1) and TO_2 line (ω_2) gives the P dependence of the mean angle $\langle\theta\rangle$ and force constant α shown in Figs. 4(e) and 4(f). The P dependence of ω_3 is then calculated using the found $\langle\theta\rangle$ and α values. It appears in accordance with the measured TO_3 frequencies [dashed lines in Fig. 4(c)] thereby strengthening the relevance of the model, at least for ω_1, ω_2, and ω_3. It is, however, worth noticing that the calculated ω_4 frequencies fall beyond those of the TO_1 mode (not accessible here).

The model predicts that for decreasing θ, ω_1 (R band) increases while ω_2 (TO_2) decreases, in line with the measurements upon Ar compression. The $\langle\theta\rangle$ value at ambient P lies a little under the admitted value ∼149°, and decreases by ∼10° as P rises to 8 GPa. The reduction of $\langle\theta\rangle$ is associated with the collapse of the large free volume of the silica network under compression [21]. Along with the reduction of $\langle\theta\rangle$, a slight increase of α by nearly 5% also occurs. The effective force constant, $\alpha \sim 600$ N/m, is in qualitative agreement with the value extracted from the Si-O interatomic force field potentials [55]. The slight increase of α with P is likely associated to a small reduction of the Si-O bond length. Such weak variations are hardly detected in diffraction experiments [17,18,56] but these are in accordance with recent simulations [57]. This analysis helps to disentangle the effects of changes in the Si-O-Si bond angle from those in the force constant. For instance, the large pressure shift of the R band results for only 10% from the rise of α, whereas 90% is due to the decrease of $\langle\theta\rangle$. On the other hand, the extremum observed for the TO_2 line at about 2 GPa turns out to be due to the balance between the α raise and $\langle\theta\rangle$ drop.

Under He pressurization, variations of Raman frequencies are considerably different. They involve a much smaller decrease, of only a couple of degrees, of the Si-O-Si angle as displayed in Fig. 4(e). This is due to He adsorption into the interstitial voids of the network [10,11] which prevents the reduction of $\langle\theta\rangle$. In contrast, the strengthening of the force constant with increasing P appears very similar to that observed under Ar compression [see Fig. 4(f)], indicating that α would be monitored by the applied fluid pressure alone, whether it is Ar or He (the additional increase above 4 GPa might be due to the steric hindrance of the adsorbed He atoms). Thus, the pressure shift of the Raman bands in He can be understood as follows. The weak positive pressure shift of the R band is evenly due to an α raise and a $\langle\theta\rangle$ drop. The increase of TO_2 frequency is in contrast mainly ascribed to the increase of α alone. This analysis shows that the overall pressure shift of the Raman bands cannot be understood solely on the basis of the intertetrahedral angle variations, without also encompassing the variations of the force constant.

Investigating silica under the two pressurizing fluids Ar and He allows varying the SiO_2 skeleton density ρ_{SiO_2} differently. For instance, compression upon 7 GPa of He or upon 2 GPa of Ar yields identical ρ_{SiO_2} (see inset in Fig. 5) [12,13]. The Raman frequencies are displayed as a function of ρ_{SiO_2} in Figs. 5(a)–5(d). All frequencies in He then appear higher than those of the sample of equivalent density compressed in Ar. The variations of $\langle\theta\rangle$ and α as a function of ρ_{SiO_2}

are also shown in Figs. 5(e) and (f), respectively. It appears that the $\langle\theta\rangle$ values in Ar and He merge into a single curve when plotted against ρ_{SiO_2}. Conversely, the variations of force constant split up. Comparing Figs. 4 and 5 shows that $\langle\theta\rangle$ scales with the SiO_2 skeleton density, whereas α mostly scales with the applied pressure. One thus concludes that, on one hand, the macroscopic volume changes are dominated by the topology of the v-SiO_2 network via the $\langle\theta\rangle$ angle alone. On the other hand, the α changes associated to the Si-O bond length variations are monitored by the applied fluid pressure alone. Our study thus reveals the role of each parameter in the compression mechanism of v-SiO_2.

Let us examine now the particular case of the D_2 line. A similar weak pressure shift is observed whether the pressurizing fluid is Ar or He. The D_2 frequency scales with the fluid pressure alone, independently of ρ_{SiO_2} as seen in Fig. 5(d). O-bending modes in threefold rings appear thus to behave differently from those of the mean effective medium. They form indeed a specific population within the network for which the angle, θ_{D_2}, and force constant, α_{D_2} are expected to differ from those of the mean medium [58].

Finally, we reanalyze in the same way a series of permanently densified samples d-SiO_2, produced by hot compression and previously investigated by Brillouin and Raman scattering [45,54]. We used two samples with ρ_{SiO_2} values of 2.46 and 2.63 g cm^{-3}, besides pristine v-SiO_2. Results are shown as black stars in Fig. 5 (the dotted lines are guides for the eye). For each d-SiO_2 sample, the $\langle\theta\rangle$ value rather matches that of the *in situ* Ar-compressed silica sample of equivalent density. This confirms again the key role of θ in governing the macroscopic volume. In contrast, the α values of the d-SiO_2 samples are much smaller than those of the *in situ* pressurized samples of equivalent densities [see Fig. 5(f)]. The lower values of α in d-SiO_2 might be evidence that the irreversible compaction process enables the glass to relax towards more favorable energetic configurations associated to less constrained SiO_4 tetrahedra than in the pristine glass.

B. Low-frequency modes

Turning to the modes at low frequency, the reduced spectra show a broadband in the 20–200 cm^{-1} frequency range associated to the so-called boson peak. Looking at Figs. 2(a) and 2(b) reveals, however, that the VV and VH components under Ar exhibit clearly different behaviors with increasing P, suggesting the existence of an additional contribution in the polarized spectra. To uncover the latter, we evaluate the spectra $\tilde{I}_{VV} = I_{VV} - I_{VH}/\rho_{BP}$ where ρ_{BP} is the depolarization ratio of boson peak modes. As the variations of ρ_{BP} with P are hardly known, the scaling factor at each P value is actually obtained assuming a vanishing $\tilde{I}_{VV}$ intensity for $\omega \to 0$. The calculated $\tilde{I}_{VV}$ spectra obtained in Ar are displayed in Fig. 6, revealing a weak component in the frequency range 100–180 cm^{-1}, over the tail of the intense polarized R band as indicated by the arrows in Fig. 6. The reliability of the existence of this weak contribution is supported by its presence on both the Stokes and anti-Stokes sides. This feature clearly separates from the R band as P increases, suggesting different origins. A similar signal is observed for v-SiO_2 pressed in He, however, less noticeable since in that case the R band does not undergo the large pressure shift and narrowing seen in Ar.

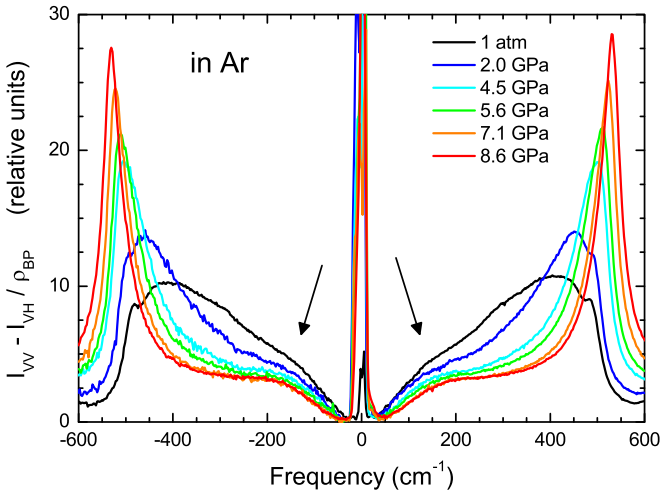

FIG. 6. . The spectra $\tilde{I}_{VV} = I_{VV} - I_{VH}/\rho_{BP}$ at some selected Ar pressures. The arrows indicate the occurrence of an additional weak isotropic component over the low-frequency tail of the R band.

The peak located around 50–70 cm^{-1} and better seen in the VH spectra is usually referred to as the boson peak. It is associated to an excess of low-frequency vibrations over the Debye level from the sound waves. It appears as a maximum in $g(\omega)/\omega^2$ where $g(\omega)$ is the vibrational density of states and it produces the anomalous bump in reduced specific heat at temperatures T around 10 K. Silica glass is one of the few materials for which the microscopic structure of the modes involved in this feature could be identified. Inelastic neutron-scattering (INS) measurements of the dynamic structure factor early suggested that they might correspond to coupled librational motions of connected rigid SiO_4 tetrahedra [59–61]. These modes are active in hyper-Raman spectroscopy [62] and produce a peak at ∼33 cm^{-1}, in accordance with INS measurements [35]. However, the origin of the signal observed in Raman light scattering at the boson peak frequency remains fundamentally unclear since the rocking of undistorted tetrahedra does not modulate the polarizability and therefore should be silent in Raman scattering [35].

To estimate the boson peak frequency ω_{BP}, we fit the reduced intensities to a log-normal function, $I_{red} \propto \exp(-\frac{[\log(\omega/\omega_{BP})]^2}{2\sigma^2})$, which is the usual approximation for its asymmetric shape. The Stokes and anti-Stokes signals are fitted simultaneously in between 25 and 150 cm^{-1}. Results for $\omega_{BP}(P)$ are shown in Figs. 7(a) and (b) for Ar and He, respectively (the spectra acquired in Ar below ∼1.3 GPa are left out of the analysis as explained in Sec. II). Our results are compared to the P variations of the longitudinal v_L and transverse v_T sound velocities measured by Brillouin scattering [12,63] and scaled to the ω_{BP} values. In Ar, one finds that $\omega_{BP}(P)$ decreases to a minimum around 2 GPa similarly to both $v_L(P)$ and $v_T(P)$. It increases thereafter, but the P variations of ω_{BP} are, however, considerably larger than those of any sound mode, and consequently of the Debye velocity, $3/v_D^3 = 1/v_L^3 + 2/v_T^3$. This rules out a simple explanation in

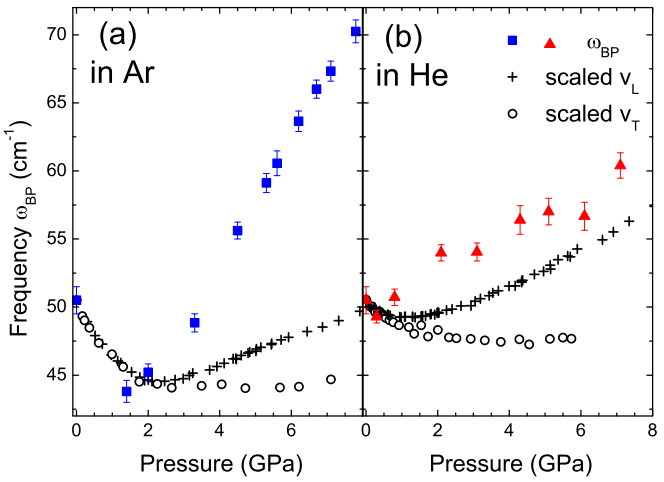

FIG. 7. Variations of the boson peak frequency ω_{BP} as a function of pressure in Ar (a) and in He (b). The crosses and circles show the longitudinal $v_L(P)$ and transverse $v_T(P)$ sound velocities [12], respectively, scaled to the ω_{BP} values. The scaling coefficients are 121 and 76 ms^{-1}/cm^{-1} for v_L and v_T, respectively.

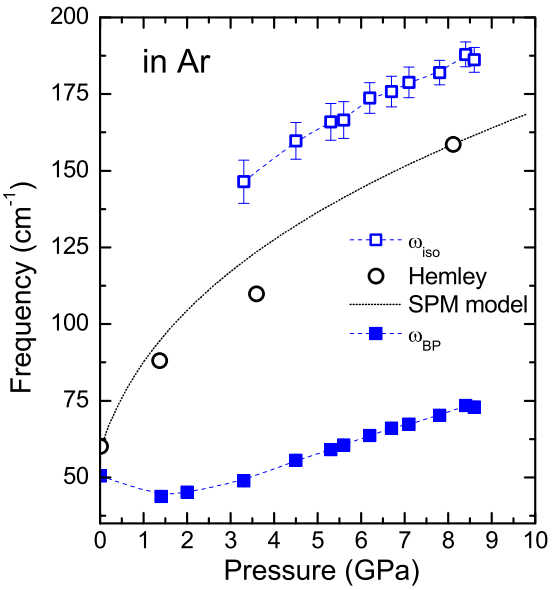

FIG. 8. The boson peak frequency ω_{BP} (filled squares) extracted from the anisotropic spectra and the additional isotropic peak frequency ω_{iso} (open squares) extracted from $\tilde{I}_{VV}$ spectra are plotted as a function of Ar pressure (the dashed lines are a guide for the eye). The data from Hemley *et al.* [22] (open circles) obtained without polarization analysis are also plotted together with the SPM model [72] (dotted line).

terms of an acoustic model described by the Debye energy alone, $E_D \propto \rho^{1/3} v_D$ [64]. A similar trend has already been reported for several polymers [65,66]. In the frame of the soft potential model (SPM), the boson peak is described in terms of quasilocalized vibrations (QLVs) [67,68]. These are soft oscillators hybridized with the sound waves, i.e., undergoing resonant coupling to acoustic waves. In silica, QLVs can be associated to the SiO_4 librational motions (responsible for the INS and hyper-Raman boson peak) coupled to the continuum of extended acoustic vibrations. Thus QLVs might be active in Raman or Brillouin light scattering. This coupling is already invoked to explain the strong acoustic damping observed in experiments at subterahertz frequencies [69]. The vibrations probed in Raman scattering at boson peak frequencies are thus expected to be the long-wavelength component of the QLVs. In this picture, $\omega_{BP}(P)$ should be driven by the P variations of the soft oscillators interacting with the acoustic continuum. Our results would thus suggest that these soft modes might get even softer at the start of compression. We have seen above that the combined changes with pressure of angle and force constant at atomic scale can produce an extremum in the frequency variations of optical modes. A possible explanation of the minimum in $\omega_{BP}(P)$ would be that the SiO_4 librational motions are modified in the same way. A direct measurement of those changes by hyper-Raman scattering would be worthwhile to check. Turning to He as pressurizing fluid, the anomalous minimum in $\omega_{BP}(P)$ disappears as shown in Fig. 7(b), in accordance with the almost suppression of the anomalies observed in He.

Defining a Grüneisen parameter as $\gamma_{BP} = \frac{\delta\omega_{BP}/\omega_{BP}}{\delta\rho/\rho}$, we estimate $\gamma_{BP} = -2.5 \pm 0.5$ at low pressure. It should be stressed that a negative Grüneisen parameter is consistent with the negative value of the thermal expansion coefficient of v-SiO_2 at low T as discussed in Refs. [70,71]. Those $\omega_{BP}(P)$ results in Ar are at variance from the ones of Hemley [22] displayed in Fig. 8 (open circles) that were extracted from unpolarized measurements. The new ω_{BP} values found here (closed squares) are much smaller. Further, they exhibit beyond the minimum, a linear pressure shift instead of the $\omega_{BP} \propto P^{1/3}$ relation [72] shown in Fig. 8 (dotted line). We estimate the Grüneisen parameter to be $\gamma_{BP} = 3.7 \pm 0.1$ in the pressure range 2–8 GPa.

Finally, as indicated above we identify in the high-frequency part of the boson peak region a new weak component which is apparent in the $\tilde{I}_{VV}$ spectra only. We estimate its frequency at the peak maximum, ω_{iso}, after subtraction of a background arising from the intense R-band tail. This background subtraction is reliable only beyond 3 GPa. The variations of ω_{iso} are plotted in Fig. 8 as a function of P (opened squares). $\omega_{iso}(P)$ is well beyond the band associated to the boson peak observed in the anisotropic spectra. This signal could be the signature of the isotropic part of the light scattered by high-frequency "acoustic" excitations as proposed by Martin and Brenig [73] or more recently by Schirmacher *et al.* [52], albeit seemingly at much too high frequency. Alternatively one notes that this signal appears in the frequency range of an intense optic mode of α-cristobalite at $\sim$115 cm^{-1}, at ambient P, active in Raman spectroscopy [74]. Interestingly, this vibration arises from the softening of a zone boundary vibration at the end of an acoustic branch in the β-cristobalite [75,76]. It turns into a zone center optic mode in the β- to α-phase transformation due to the doubling of the unit cell and thus becomes Raman active. Therefore, the signal ω_{iso} of the glass could be, on one hand, the counterpart of this low-frequency optic mode which would appear strongly broadened by disorder. It might, however, also result from incoherent scattering by the zone boundary mode in β-cristobalite induced by disorder of the glass.

V. CONCLUSION AND OUTLOOK

A comprehensive picture of the pressure and density dependencies of Raman-active vibrational modes of v-SiO_2 is proposed. New accurate data, including polarization analysis, are collected throughout the elastic domain of the glass, i.e., the 0–8 GPa range associated to about 0%–25% of compaction rate, in which all the structural modifications are fully reversible. *In situ* experiments under hydrostatic pressure are performed using two distinct rare gases as pressurizing media: Ar and He. Owing to its much smaller size, He atoms largely penetrate into the free volume of the glass network resulting in a reduced compaction rate.

The vibrational spectra are examined on the basis of a well-known central-force model for dynamics of tetrahedral networks relating the Raman mode frequencies to the force constant and the intertetrahedral angle of the Si-O-Si bonds. The compression mechanism of v-SiO_2 is thought to take place mainly by reduction of the bridging oxygen angle, with negligible change in the force constant. We show here that variations of both parameters are actually needed to account for the vibrational frequency changes of compacted samples. For example, the faint maximum observed for the TO_2 mode frequency at about 2 GPa of Ar pressure results from the balance between the stiffening of the force constant and the shrinking of the intertetrahedral angle. The latter appears to be driven by the sample density only, a result confirmed by data obtained on the permanently densified samples. Conversely, the mean force constant smoothly increases with the applied pressure. The latter variations arise from the elastic strains sustained by the tetrahedra upon loading. Remarkably, the densified samples exhibit lower force constants than a pristine sample indicating that the high-temperature densification process would allow residual strain relaxation. The overall results open up new possibilities for understanding the relation between the thermomechanical history and microstructure of vitreous silica [77].

Furthermore, a careful polarization analysis of the low-frequency part of the spectra reveals that the heretofore P dependence of the Raman boson peak of vitreous silica was ill-resolved, owing to the mixing with a broad higher frequency component. The latter, active in the isotropic spectrum only, is tentatively ascribed to an optic mode also active in the Raman spectrum of α-cristobalite in the same frequency range. The new pressure dependence of the Raman boson peak of vitreous silica is much weaker than previously known, though it still cannot be reconciled with any sound velocity variation within a simple picture. Finally, the boson peak frequency shows a faint minimum around 2 GPa, in coincidence with the well-known compressibility maximum of vitreous silica, demonstrating that acoustic and boson peak modes are both sensitive to the overall pressure-induced microscopic changes.

ACKNOWLEDGMENTS

The authors thank G. Prévot for technical support, C. Dupas for the sample preparation, and G. LeMarchand for his help in DAC loading. This work was supported by the French National Research Agency program MECASIL ANR-12-BS04-0004-03; it was also partially funded by Région Languedoc-Roussillon (Omega Platform).

[1] S. Susman, K. J. Volin, D. L. Price, M. Grimsditch, J. P. Rino, R. K. Kalia, P. Vashishta, G. Gwanmesia, Y. Wang, and R. C. Liebermann, Phys. Rev. B **43**, 1194 (1991).
[2] A. Polian and M. Grimsditch, Phys. Rev. B **41**, 6086 (1990).
[3] C. S. Zha, R. J. Hemley, H.-k. Mao, T. S. Duffy, and C. Meade, Phys. Rev. B **50**, 13105 (1994).
[4] L. Huang and J. Kieffer, Phys. Rev. B **69**, 224203 (2004).
[5] Y. Liang, C. R. Miranda, and S. Scandolo, Phys. Rev. B **75**, 024205 (2007).
[6] A. Walker, L. Sullivan, K. Trachenko, R. Bruin, T. White, M. Dove, R. Tyer, I. Todorov, and S. Wells, J. Phys.: Condens. Matter **19**, 275210 (2007).
[7] B. Mantisi, A. Tanguy, G. Kermouche, and E. Barthel, Eur. Phys. J. B **85**, 1 (2012).
[8] B. Mantisi, G. Kermouche, E. Barthel, and A. Tanguy, Phys. Rev. E **93**, 033001 (2016).
[9] J. Shelby, J. Appl. Phys. **47**, 135 (1976).
[10] T. Sato, N. Funamori, and T. Yagi, Nat. Commun. **2**, 345 (2011).
[11] G. Shen, Q. Mei, V. Prakapenka, P. Lazor, S. Sinogeikin, Y. Meng, and C. Park, Proc. Natl. Acad. Sci. USA **108**, 6004 (2011).
[12] C. Weigel, A. Polian, M. Kint, B. Rufflé, M. Foret, and R. Vacher, Phys. Rev. Lett. **109**, 245504 (2012).
[13] B. Coasne, C. Weigel, A. Polian, M. Kint, J. Rouquette, J. Haines, M. Foret, R. Vacher, and B. Rufflé, J. Phys. Chem. B **118**, 14519 (2014).
[14] K. Trachenko, M. T. Dove, V. Brazhkin, and F. S. El'kin, Phys. Rev. Lett. **93**, 135502 (2004).
[15] T. Rouxel, H. Ji, T. Hammouda, and A. Moréac, Phys. Rev. Lett. **100**, 225501 (2008).
[16] K. Trachenko and M. T. Dove, Phys. Rev. B **67**, 064107 (2003).
[17] C. J. Benmore, E. Soignard, S. A. Amin, M. Guthrie, S. D. Shastri, P. L. Lee, and J. L. Yarger, Phys. Rev. B **81**, 054105 (2010).
[18] A. Zeidler, K. Wezka, R. F. Rowlands, D. A. J. Whittaker, P. S. Salmon, A. Polidori, J. W. E. Drewitt, S. Klotz, H. E. Fischer, M. C. Wilding, C. L. Bull, M. G. Tucker, and M. Wilson, Phys. Rev. Lett. **113**, 135501 (2014).
[19] D. Wakabayashi, N. Funamori, T. Sato, and T. Taniguchi, Phys. Rev. B **84**, 144103 (2011).
[20] P. N. Sen and M. F. Thorpe, Phys. Rev. B **15**, 4030 (1977).
[21] R. J. Hemley, H. K. Mao, P. M. Bell, and B. O. Mysen, Phys. Rev. Lett. **57**, 747 (1986).
[22] R. J. Hemley, C. Meade, and H.-k. Mao, Phys. Rev. Lett. **79**, 1420 (1997).
[23] T. Deschamps, C. Martinet, D. Neuville, D. de Ligny, C. Coussa-Simon, and B. Champagnon, J. Non-Cryst. Solids **355**, 2422 (2009).
[24] J. C. Chervin, B. Canny, J. M. Besson, and P. Pruzan, Rev. Sci. Instrum. **66**, 2595 (1995).
[25] J. C. Chervin, B. Canny, and M. Mancinelli, High Press. Res. **21**, 305 (2001).

[26] S. Solin and A. Ramdas, Phys. Rev. B **1**, 1687 (1970).
[27] S. Klotz, J.-C. Chervin, P. Munsh, and G. Le Marchand, J. Phys. D: Appl. Phys. **42**, 075413 (2009).
[28] G. H. Watson, Jr. and W. B. Daniels, Physica B+C **139-140**, 472 (1986).
[29] W. Hayes and R. Loudon, *Scattering of Light by Crystals* (Dover, New York, 1978 and 2004 editions).
[30] R. Shuker and R. W. Gammon, Phys. Rev. Lett. **25**, 222 (1970).
[31] F. L. Galeener and P. N. Sen, Phys. Rev. B **17**, 1928 (1978).
[32] P. Umari, X. Gonze, and A. Pasquarello, Phys. Rev. Lett. **90**, 027401 (2003).
[33] F. L. Galeener and G. Lucovsky, Phys. Rev. Lett. **37**, 1474 (1976).
[34] F. L. Galeener, A. J. Leadbetter, and M. W. Stringfellow, Phys. Rev. B **27**, 1052 (1983).
[35] B. Hehlen and G. Simon, J. Raman Spectrosc. **43**, 1941 (2012).
[36] S. N. Taraskin and S. R. Elliott, Phys. Rev. B **56**, 8605 (1997).
[37] F. Galeener, Solid State Commun. **44**, 1037 (1982).
[38] A. Pasquarello and R. Car, Phys. Rev. Lett. **80**, 5145 (1998).
[39] F. L. Galeener, Phys. Rev. B **19**, 4292 (1979).
[40] L. Giacomazzi, P. Umari, and A. Pasquarello, Phys. Rev. B **79**, 064202 (2009).
[41] Q. Mei, C. J. Benmore, S. Sen, R. Sharma, and J. L. Yarger, Phys. Rev. B **78**, 144204 (2008).
[42] S. Kohara and K. Suzuya, J. Phys.: Condens. Matter **17**, S77 (2005).
[43] F. Mauri, A. Pasquarello, B. G. Pfrommer, Y.-G. Yoon, and S. G. Louie, Phys. Rev. B **62**, R4786 (2000).
[44] A. Rahmani, M. Benoit, and C. Benoit, Phys. Rev. B **68**, 184202 (2003).
[45] B. Hehlen, J. Phys.: Condens. Matter **22**, 025401 (2010).
[46] E. Courtens, M. Foret, B. Hehlen, and R. Vacher, Solid State Commun. **117**, 187 (2001).
[47] M. Wilson, P. A. Madden, M. Hemmati, and C. A. Angell, Phys. Rev. Lett. **77**, 4023 (1996).
[48] V. K. Malinovsky and A. P. Sokolov, Solid State Commun. **57**, 757 (1986).
[49] N. V. Surovtsev and A. P. Sokolov, Phys. Rev. B **66**, 054205 (2002).
[50] A. Fontana, F. Rossi, and E. Fabiani, J. Non-Cryst. Solids **352**, 4601 (2006).
[51] B. Schmid and W. Schirmacher, Phys. Rev. Lett. **100**, 137402 (2008).
[52] W. Schirmacher, T. Scopigno, and G. Ruocco, J. Non-Cryst. Solids **407**, 133 (2015).
[53] M. F. Thorpe and F. L. Galeener, Phys. Rev. B **22**, 3078 (1980).
[54] E. Rat, M. Foret, G. Massiera, R. Vialla, M. Arai, R. Vacher, and E. Courtens, Phys. Rev. B **72**, 214204 (2005).
[55] A. Carré, J. Horbach, S. Ispas, and W. Kob, Europhys. Lett. **82**, 17001 (2008).
[56] C. Meade, R. J. Hemley, and H. K. Mao, Phys. Rev. Lett. **69**, 1387 (1992).
[57] S. Ispas (private communication).
[58] F. L. Galeener, R. A. Barrio, E. Martinez, and R. J. Elliott, Phys. Rev. Lett. **53**, 2429 (1984).
[59] U. Buchenau, N. Nücker, and A. J. Dianoux, Phys. Rev. Lett. **53**, 2316 (1984).
[60] U. Buchenau, M. Prager, N. Nücker, A. J. Dianoux, N. Ahmad, and W. A. Phillips, Phys. Rev. B **34**, 5665 (1986).
[61] E. Fabiani, A. Fontana, and U. Buchenau, J. Chem. Phys. **128**, 244507 (2008).
[62] B. Hehlen, E. Courtens, R. Vacher, A. Yamanaka, M. Kataoka, and K. Inoue, Phys. Rev. Lett. **84**, 5355 (2000).
[63] S. Ayrinhac, B. Rufflé, M. Foret, H. Tran, S. Clément, R. Vialla, R. Vacher, J. C. Chervin, P. Munsch, and A. Polian, Phys. Rev. B **84**, 024201 (2011).
[64] B. Rufflé, S. Ayrinhac, E. Courtens, R. Vacher, M. Foret, A. Wischnewski, and U. Buchenau, Phys. Rev. Lett. **104**, 067402 (2010).
[65] K. Niss, B. Begen, B. Frick, J. Ollivier, A. Beraud, A. Sokolov, V. N. Novikov, and C. Alba-Simionesco, Phys. Rev. Lett. **99**, 055502 (2007).
[66] L. Hong, B. Begen, A. Kisliuk, C. Alba-Simionesco, V. N. Novikov, and A. P. Sokolov, Phys. Rev. B **78**, 134201 (2008).
[67] D. A. Parshin, Phys. Solid State **36**, 991 (1994).
[68] D. A. Parshin, H. R. Schober, and V. L. Gurevich, Phys. Rev. B **76**, 064206 (2007).
[69] B. Rufflé, D. A. Parshin, E. Courtens, and R. Vacher, Phys. Rev. Lett. **100**, 015501 (2008).
[70] H. R. Schober, U. Buchenau, and V. L. Gurevich, Phys. Rev. B **89**, 014204 (2014).
[71] G. K. White, S. J. Collocott, and J. S. Cook, Phys. Rev. B **29**, 4778 (1984).
[72] V. L. Gurevich, D. A. Parshin, and H. R. Schober, Phys. Rev. B **71**, 014209 (2005).
[73] A. J. Martin and W. Brenig, Phys. Status Solidi B **64**, 163 (1974).
[74] V. N. Sigaev, E. N. Smelyanskaya, V. G. Plotnichenko, V. V. Koltashev, A. A. Volkov, and P. Pernice, J. Non-Cryst. Solids **248**, 141 (1999).
[75] I. P. Swainson, M. T. Dove, and D. C. Palmer, Phys. Chem. Miner. **30**, 353 (2003).
[76] J. Etchepare, M. Merian, and P. Kaplan, J. Chem. Phys. **68**, 1531 (1978).
[77] M. Guerette, M. R. Ackerson, J. Thomas, F. Yuan, E. B. Watson, D. Walker, and L. Huang, Sci. Rep. **5**, 15343 (2015).